Title

BiP/GRP78 is a pro-viral factor for diverse dsDNA viruses that promotes the survival and proliferation of cells upon KSHV infection.

Journal

PLoS Pathogens, 20(10)

Authors

Najarro, Guillermo
Brackett, Kevin
Woosley, Hunter
et al.

Publication Date

2024-10-29

DOI

10.1371/journal.ppat.1012660

Peer reviewed

PLOS PATHOGENS

RESEARCH ARTICLE

BiP/GRP78 is a pro-viral factor for diverse dsDNA viruses that promotes the survival and proliferation of cells upon KSHV infection

Guillermo Najarro[1], Kevin Brackett[1], Hunter Woosley[2], Leah C. Dorman[2], Vincent Turon-Lagot[2], Sudip Khadka[2], Catya Faeldonea[1], Osvaldo Kevin Moreno[1], Adriana Ramirez Negron[1], Christina Love[3], Ryan Ward[3], Charles Langelier[2,3], Frank McCarthy[2], Carlos Gonzalez[2], Joshua E. Elias[2], Brooke M. Gardner[1], Carolina Arias[1,2]*

1 University of California, Santa Barbara, California, United States of America, **2** Chan Zuckerberg BioHub, San Francisco, California, United States of America, **3** Department of Medicine, University of California, San Francisco, California, United States of America

* Carolina.arias@czbiohub.org

Citation: Najarro G, Brackett K, Woosley H, Dorman LC, Turon-Lagot V, Khadka S, et al. (2024) BiP/GRP78 is a pro-viral factor for diverse dsDNA viruses that promotes the survival and proliferation of cells upon KSHV infection. PLoS Pathog 20(10): e1012660. https://doi.org/10.1371/journal.ppat.1012660

Editor: Laurie T. Krug, National Cancer Institute, UNITED STATES OF AMERICA

Received: July 26, 2024

Accepted: October 11, 2024

Published: October 29, 2024

Data Availability Statement: The RNA-seq data and the code used in this study were uploaded to the GEO database with the accession number GSE 280006.

Funding: This work was supported by a grant to CA from the University of California Research Initiatives (UCRI CTN-19-586108). GN was supported by the National Science Foundation (NSF) Bridge to Doctorate. HW, LD, VT-L, SK, CL, RW, CL, CG, FMC, JEE, and CA were supported by

Abstract

The Endoplasmic Reticulum (ER)-resident HSP70 chaperone BiP (HSPA5) plays a crucial role in maintaining and restoring protein folding homeostasis in the ER. BiP's function is often dysregulated in cancer and virus-infected cells, conferring pro-oncogenic and pro-viral advantages. We explored BiP's functions during infection by the Kaposi's sarcoma-associated herpesvirus (KSHV), an oncogenic gamma-herpesvirus associated with cancers of immunocompromised patients. Our findings reveal that BiP protein levels are upregulated in infected epithelial cells during the lytic phase of KSHV infection. This upregulation occurs independently of the unfolded protein response (UPR), a major signaling pathway that regulates BiP availability. Genetic and pharmacological inhibition of BiP halts KSHV viral replication and reduces the proliferation and survival of KSHV-infected cells. Notably, inhibition of BiP limits the spread of other alpha- and beta-herpesviruses and poxviruses with minimal toxicity for normal cells. Our work suggests that BiP is a potential target for developing broad-spectrum antiviral therapies against double-stranded DNA viruses and a promising candidate for therapeutic intervention in KSHV-related malignancies.

Author summary

The endoplasmic reticulum (ER) chaperone protein BiP (HSPA5) plays a central role in protein folding and maintaining homeostasis within the ER. Under certain conditions, such as cancer and viral infections, BiP is dysregulated to support cell survival or viral replication. In this study, we investigated the regulation and requirement of BiP during infection by Kaposi's sarcoma-associated herpesvirus (KSHV), an oncogenic herpesvirus linked to cancers in immunocompromised individuals. Our findings demonstrate that BiP is significantly upregulated in KSHV-infected cells, even when the expression of most other cellular genes is suppressed. Notably, the function of BiP is essential for KSHV replication and the survival of KSHV-infected cells. This reliance on BiP is not unique to

the Chan Zuckerberg Biohub intramural program. The funders had no role in study design, data collection and analysis, decision to publish, or preparation of the manuscript.

Competing interests: The authors have declared that no competing interests exist.

KSHV; it is also required for the replication of other double-stranded DNA (dsDNA) viruses, including Herpes simplex virus I, Human Cytomegalovirus, and Vaccinia Virus. These findings underscore the critical role of BiP in dsDNA viral infections, positioning this chaperone as a promising target for the development of broad-spectrum antiviral therapies and potential treatment strategies for KSHV-associated malignancies.

Introduction

Viruses dramatically remodel cellular physiology to accommodate the heightened biosynthetic demand for generating new viral particles. This process is orchestrated by virus-encoded factors that subvert the host protein homeostasis (proteostasis) machinery to promote the timely and optimal synthesis, folding, and maturation of proteins required for viral replication [1,2]. Among the hundreds of proteostasis factors, molecular chaperones are critical for viral infections [2–5].

Molecular chaperones assist in folding, refolding, and translocating nascent, unfolded, or misfolded proteins to promote the acquisition of functional conformations or target terminally misfolded proteins for degradation, thus maintaining proteome integrity [6,7]. Viruses co-opt host chaperones, especially those belonging to the heat shock protein (HSP) family, by altering the levels, interactions, or localization of HSPs to facilitate viral entry and replication, viral protein synthesis, and virion assembly [2,3]. While all viruses exploit the function of chaperones in different cellular compartments, enveloped viruses, which are surrounded by an outer lipid layer acquired from the host and encode one or more glycoproteins, heavily rely on endoplasmic reticulum (ER) chaperones [5,8].

The ER is a membrane-bound organelle where most transmembrane and secretory proteins are synthesized, folded, and modified [9]. A master regulator of ER functions is the Binding immunoglobulin protein/Glucose-regulated protein 78 (BiP/GRP78), an ER-resident HSP70 that assists nascent peptide folding [10]. BiP is also a key player in the unfolded protein response (UPR), the ER stress response [11–13]. BiP modulates the activity of the three transmembrane ER stress sensor proteins governing the UPR. These sensors are the kinase/nuclease IRE1, the kinase PERK, and the ER-membrane tethered transcription factor ATF6 [14,15]. When the cell's biosynthetic output surpasses the ER's folding capacity, unfolded proteins accumulate in the ER lumen, which licenses the activation of IRE1, PERK, and ATF6 through well-described mechanisms involving their reversible dissociation from BiP, direct activation by unfolded protein ligands, or changes in the redox status of the ER lumen. The signaling cascade downstream of the sensors culminates in the activation of gene expression programs that restore ER homeostasis (reviewed in [16]).

In virus-infected cells, BiP is upregulated by flaviviruses (Zika, ZIKV; and Dengue, DENV virus), coronaviruses (SARS-CoV-2, MERS-CoV), Hepatitis B Virus (HBV), and Human Cytomegalovirus (HCMV), a member of the betaherpesvirus subfamily [17–21]. Pharmacological inhibition or knockdown of BiP reduces viral replication in cultured cells (ZIKV, DENV, SARS-CoV-2, and HCMV) and mouse infection models (SARS-CoV-2), highlighting its pro-viral activity.

Beyond viral infection, BiP is elevated in numerous cancers, including leukemia, melanoma, multiple myeloma, brain, pancreatic, liver, and breast cancer, and is regarded as a promising biomarker and therapeutic target in several diseases [22]. In addition to heightened levels, BiP can re-localize to the cell surface during ER stress, which correlates with tumor aggressiveness and poor prognosis [23,24]. Moreover, BiP protects cancer cells from apoptosis

and promotes proliferation and metastasis, thereby contributing to tumor robustness and resistance to therapy [22,25].

Motivated by these observations, we investigated the roles of BiP during infection by the oncogenic gamma-herpesvirus Kaposi's Sarcoma-Associated Herpesvirus (KSHV). KSHV is the most recently discovered human herpesvirus and the causal agent of Kaposi's sarcoma (KS), the lymphoproliferative disorders Primary Effusion Lymphoma (PEL), and KSHV-associated multicentric Castleman's disease (MCD), and is implicated in KSHV inflammatory cytokine syndrome (KICS) [26,27]. Few treatment options are available for these diseases, and an unmet clinical need exists for a targeted antiviral therapeutic [27].

KSHV contains a ~160Kb double-stranded DNA genome that encodes over 80 proteins [28, 29]. As with all other herpesviruses, KSHV establishes life-long latent infections characterized by the expression of a few viral products. To complete its life cycle, KSHV reactivates from this latent state to a lytic, virion-productive infection characterized by a massive induction of viral transcripts and protein synthesis [29,30]. KSHV is an enveloped virus, and several of its proteins are synthesized in the ER [31]; therefore, KSHV infection could impose a high biosynthetic burden on this organelle.

Here, we show that BiP is upregulated during KSHV lytic infection, independent of UPR activation, and acts as a pro-viral factor for multiple types of DNA viruses (herpes and poxviruses), underscoring that inhibiting BiP may provide broad-spectrum antiviral utility. Moreover, we report that BiP inhibition with the thiazole benzenesulfonamide HA15 has strong cytostatic and cytotoxic effects in KSHV-infected B-cells and primary endothelial cells but not in uninfected cells, supporting the notion that BiP inhibition is a promising therapeutic alternative for KSHV-associated malignancies.

Results

BiP is upregulated during the lytic cycle of KSHV in iSLK.219 cells

KSHV encodes at least 14 transmembrane or secreted proteins with functions in cell entry, viral gene expression, and immune evasion (Table 1). These viral proteins are folded, processed, and assembled in the ER with the assistance of cellular chaperones. To investigate the role of BiP during the lytic cycle of KSHV, we used the well-established iSLK.219 model system to study KSHV reactivation [32]. iSLK.219 cells are latently infected with KSHV and contain a doxycycline (Dox)-inducible viral transcription factor RTA (replication and transcriptional activator), the expression of which is sufficient to induce entry to the KSHV's lytic cycle (Fig 1A). iSLK.219s harbor KSHV.219, a recombinant virus that encodes a constitutive GFP reporter and an RTA-inducible RFP reporter in the viral genome that facilitates monitoring infection and viral reactivation (S1A and S1B Fig) [33]. We induced iSLK.219 cells with Dox and collected cell lysates at 0h, 24h, 48h, and 72h, representing the latent (0h), early-lytic (24h-48h), and late-lytic (48h-72h) stages of infection, and monitored the levels of BiP by immunoblot throughout a time course of reactivation (Fig 1B). Protein levels of BiP significantly increased early in the lytic cycle of KSHV, starting at 24h post-reactivation, and coincide with an upsurge in viral protein expression (Figs 1B and S1B). To determine the timing of BiP upregulation during the lytic cycle, we used the viral DNA replication inhibitor phosphonoformate (PFA), which arrests infection in the early stages of the lytic cycle by preventing viral DNA replication (Fig 1C) [34]. The levels of BiP in iSLK.219 cells induced with Dox for 72h were indistinguishable in PFA-treated from untreated cells, indicating that the upregulation of BiP is an early event in the viral lytic cycle that is independent of late viral gene expression (Fig 1C). Notably, we did not detect any changes in the levels of GRP94 or Calreticulin—two prominent

Table 1. KSHV proteins containing signal peptides.

Gene Name	Function	Time of Expression	Signal Peptide	Transmembrane domains
K1	Glycoprotein	Latent	1–18	224–247
ORF4	Complement Binding Protein	Early	1–19	533–551
ORF8	Glycoprotein B	Late	1–26	743–762
K2	Viral Interleukin 6 Homologue	Latent	1–22	N/A
K4	v-Macrophage Inflammatory Protein 2	Immediate Early	1–25	N/A
K4.1	v-Macrophage Inflammatory Protein 3	Immediate Early	1–27	N/A
K6	v-Macrophage Inflammatory Protein 1	Immediate Early	1–24	N/A
ORF22	Glycoprotein H	Late	1–21	715–736
ORF39	Glycoprotein M	Early	1–29	14–25, 79–103, 119–135, 153–171, 211–231, 240–260, 274–293, 307–325
ORF47	Glycoprotein L	Early	1–20	N/A
K8.1	Glycoprotein	Late	1–26	200–220
ORF53	Glycoprotein N	Late	1–23	79–99
K14	Viral OX2	Early	1–24	230–250
K15	LMP1/2 Homologue	Latent/Early	1–25	10–25, 35–50, 69–81, 91–100, 123–139, 150–167, 178–194, 207–223, 240–250, 272–287, 299–308, 329–349

The protein sequences of all annotated KSHV proteins (GQ994935.1) were analyzed with the signal sequence prediction engines Phobius [35], Signal P 6.0 [36], and Predisi [37]. Signal peptides (SP) were annotated if predicted by two or more engines. The transmembrane domains of proteins containing SPs were annotated using DeepTMHMM [38].

https://doi.org/10.1371/journal.ppat.1012660.t001

ER chaperones—during the lytic cycle of KSHV, suggesting that the upregulation of BiP during infection is not general to all ER chaperones (Fig 1D).

BiP upregulation during the early-lytic cycle of KSHV is independent of the UPR

BiP mRNA levels are increased by the UPR transcription factors XBP1s and ATF6 in response to ER stress to allow homeostatic readjustment [13,39]. qRT-PCR analyses revealed that KSHV lytic infection did not coincide with an increase in BiP mRNA levels (Fig 1E), suggesting post-transcriptional BiP upregulation in our experiments that is likely independent of UPR induction during infection. Previous reports indicate that KSHV modulates the UPR in PEL-derived cells by disrupting signal transduction downstream of the UPR sensors IRE1, PERK, and ATF6 [40]. To determine whether the UPR is dysregulated during KSHV infection in iSLK.219 cells, we measured the levels, phosphorylation status, and activity of IRE1 during viral reactivation (Fig 2A). Phosphorylated IRE1 (IRE1-P) levels increased as the lytic cycle progressed. Despite the evident activation of IRE1 during the lytic cycle of KSHV, we observed a minimal XBP1 mRNA splicing (XBP1s) and XBP1s protein, a direct product of IRE1 activity, indicating disruption of canonical IRE1 signaling during lytic infection in iSLK.219 cells (Fig 2A-2C).

Even though XBP1s was barely detectable during the KSHV lytic cycle in iSLK.219 cells, we tested whether the low levels of this potent UPR transcription factor could mediate the upregulation of BiP. To this end, we used CRISPRi-mediated gene silencing of XBP1 (Fig 2D) [41] and found that the knockdown of XBP1 did not significantly impact BiP protein levels or viral production in iSLK.219 cells (Fig 2D and 2E). In parallel, we investigated whether ATF6 was

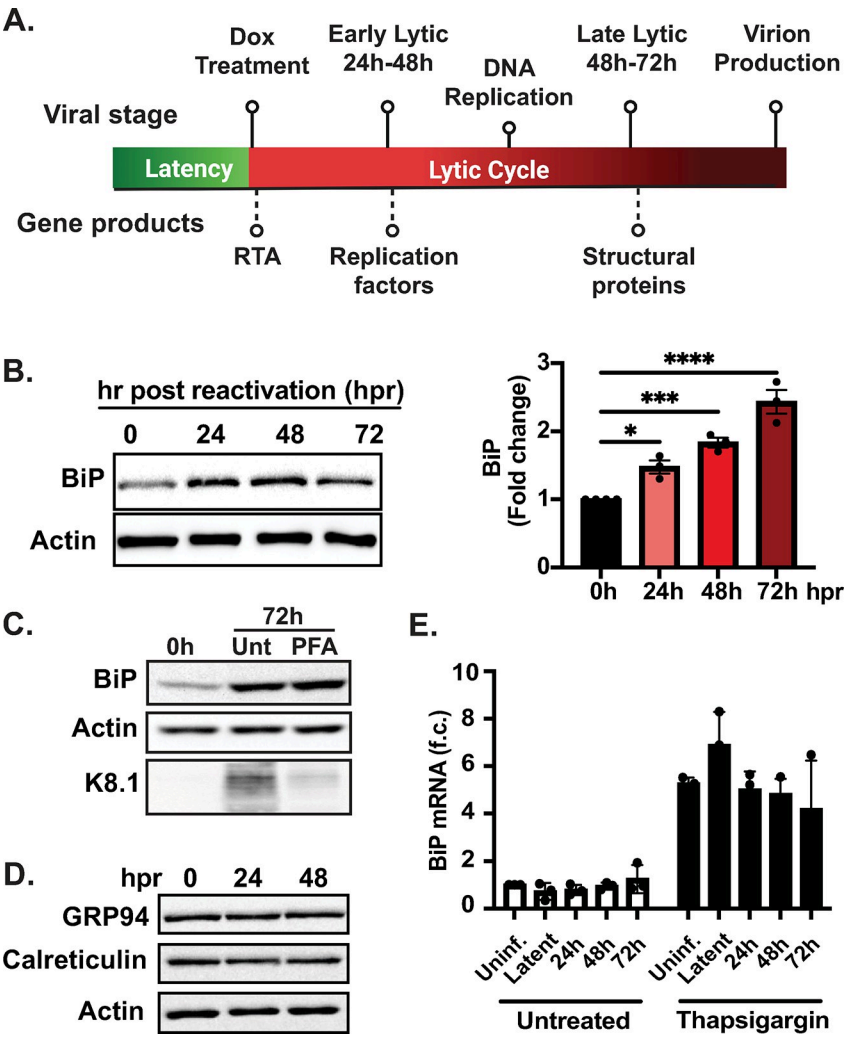

Fig 1. BiP is upregulated during the KSHV lytic cycle. (A) Schematic of lytic reactivation in iSLK.219 cells **(B)** BiP is upregulated at the protein level in a time course of reactivation. (Left) iSLK.219 cells were treated with Dox (1 μg/ml) to induce RTA expression and viral reactivation. Whole-cell lysates collected at the indicated times were analyzed by immunoblot. Actin: loading control. (Right) Image densitometry quantification of the immunoblot **(C)** BiP upregulation is independent of late viral gene expression. Viral DNA replication was inhibited in iSLK.219 cells by pretreatment with PFA (100 nM) for 24h before induction with Dox. Whole-cell lysates collected at the indicated times were analyzed by immunoblot. Actin: loading control. **(D)** Immunoblot of GRP94, calreticulin, and actin during KSHV reactivation in iSLK.219 cells **(E)** BiP upregulation is post-transcriptional. qRT-PCR quantification of BiP mRNA in a time course of reactivation in iSLK.219 untreated or treated with Tg (100nM) for 4h. Note the high levels of BiP mRNA in cells undergoing acute ER stress. $N = 3$ independent biological replicates for (B, C, D, and E). Values in (B, E) are average ±SEM. Statistical significance in (B) was calculated using a one-way ANOVA (*P = 0.01, **P = 0.004, **P = <0.0001).

https://doi.org/10.1371/journal.ppat.1012660.g001

responsible for the upregulation of BiP observed during KSHV lytic infection. We depleted ATF6 using CRISPRi or inhibited its activation with the ATF6 inhibitor CeapinA7, a small molecule that blocks ATF6 ER export [42]. Neither CeapinA7 treatment nor ATF6 knockdown by CRISPRi affected the accumulation of BiP protein or the production of infectious virus in iSLK.219 cells undergoing KSHV lytic infection (Fig 2F-2H). These findings indicate that KSHV reactivation exerts UPR-independent, post-transcriptional BiP protein upregulation in these cells (Fig 2D, 2F and 2G).

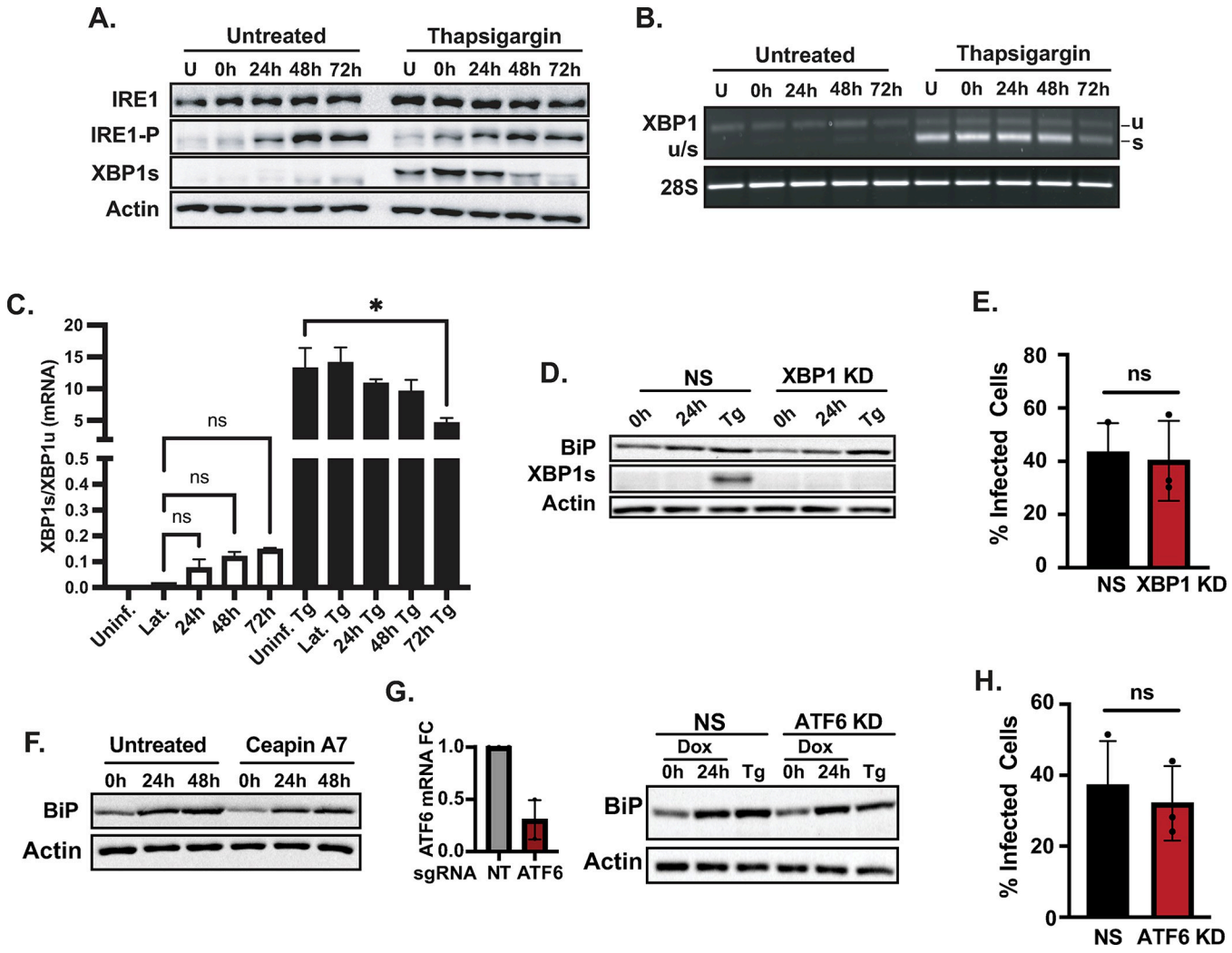

Fig 2. BiP is post-transcriptionally upregulated independently of ATF6 and XBP1. (A-C) IRE1 is phosphorylated in lytic iSLK.219 cells without detectable XBP1 splicing. Cells were reactivated by treatment with Dox (1 μg/ml). At the indicated times, the cells were treated with Tg (100 nM) for 4h to induce acute ER stress. **(A)** Whole-cell lysates were collected and analyzed by immunoblot for total (IRE1) or phosphorylated IRE1 (IRE1-P), spliced XBP1 (XBP1s), and actin (loading control). **(B)** RT-PCR detection of unspliced (u) and spliced (s) XBP1 mRNA. **(C)** Image densitometry quantification of the data in (B). **(D-H)** XBP1 and ATF6 are not required for BiP protein upregulation or infectious virus production during the KSHV lytic cycle. **(D)** CRISPRi-based knockdown of XBP1 (XBP1-KD) in iSLK.219-dCas9 cells. Cells (NS and XBP1-KD) were induced with Dox (1 μg/ml) for 24h. Cells were treated with Tg (100 nM) for 4h before collection. Whole-cell lysates were analyzed by immunoblot. Actin: loading control. **(E)** The supernatants of cells treated as in (D) were collected and used to spinoculate uninfected iSLK cells. The percent of GFP expression was determined by automated cell counting and used as a proxy for infectious virus levels in the supernatants. **(F)** iSLK.219 cells were treated with the ATF6 inhibitor CeapinA7 (6 μM) for 2h before induction with Dox (1 μg/ml). Whole-cell lysates were collected at the indicated times and analyzed by immunoblot. **(G)** CRISPRi-based knockdown of ATF6 (ATF6KD) in iSLK.219-dCas9 cells. ATF6-KD cells were treated as in (D). The knockdown of ATF6 expression was determined by qRT-PCR. **(H)** Supernatants from ATF6-KD cells were collected and processed as described in (E). *N* = 3 independent biological replicates. Values in (C, E, F) are average ±SEM. Statistical significance was calculated using a one-way ANOVA (*P = 0.01) in (C) or a paired t-test (E and H).

https://doi.org/10.1371/journal.ppat.1012660.g002

BiP upregulation could result from the recruitment of alternative translation initiation factors during infection. Indeed, eIF2A is one factor reported to promote BiP expression under acute ER stress [43]. eIF2A mediates binding of the Met-tRNAi to the 40S subunit under stress conditions when eIF2a-Met-tRNAi-GTP availability is restricted. Small interfering RNA (siRNA) silencing of eIF2A in iSLK.219 cells enhanced the expression of BiP in latent and lytic cells compared to control cells, indicating that in the context of KSHV-infected cells, eIF2A behaves as a suppressor rather than a promoter of BiP expression (S2 Fig).

BiP is a pro-viral factor in KSHV-infected cells

The upregulation of BiP protein during KSHV lytic infection in iSLK.219 cells is remarkable given the substantial host shutoff mediated by the KSHV SOX (shutoff and exonuclease) protein, which degrades host mRNAs. This viral factor suppresses the expression of host proteins to funnel host cell resources towards the pathogen's benefit [44]. Because this result suggests BiP effectively escapes host shutoff in iSLK.219 cells, we tested whether KSHV exploits BiP during its lytic cycle. To this end, we used HA15, a thiazole benzenesulfonamide inhibitor of BiP that targets its ATPase domain [45]. Treatment of iSLK.219 cells with HA15 had a striking effect on KSHV reactivation by reducing lytic protein expression and decreasing infectious virus production by up to 90% without causing cytotoxicity (Figs 3A and 3B, S3A). In an orthogonal approach, we silenced BiP expression by siRNA-mediated knockdown. BiP's genetic depletion phenocopied HA15 treatment and significantly reduced viral protein expression and infectious virus production (Fig 3C and 3D), thus corroborating that BiP is essential for KSHV replication in these cells. Importantly, HA15 treatment does not alter the maintenance of latent viral genomes, as measured by the expression of the episome-encoded GFP, or transcriptional activity of the dox-induced RTA, which initiates the lytic cycle in iSLK.219 cells (S3B and S3C Fig). Additionally, BiP inhibition in naïve iSLK cells does not reduce the efficiency of KSHV *de novo* infection and establishment of latency (S3D Fig). To determine if the observed effect of HA15 on KSHV reactivation was restricted to iSLK.219 cells, we investigated its impact on the inducible B-cell lymphoma-derived cell line TREx-BCBL1-RTA, which is also latently infected with KSHV and expresses RTA under the control of a doxycycline-inducible promoter [46]. Interestingly, in TREx-BCBL-1 cells, we did not detect an upsurge in BiP protein levels during the KSHV lytic cycle (S4 Fig). Despite this observation, treatment of TREx-BCBL-1-RTA cells with HA15 during a time course of lytic reactivation with Dox reduced viral protein expression and viral DNA replication comparable to the effect observed in iSLK.219s treated with HA15 (Fig 3E and 3F). These observations confirm that BiP is a pro-viral factor during KSHV lytic infection in multiple infection models and cell types.

BiP inhibition disrupts the early stages of the KSHV lytic cycle

Our observations suggested that blocking BiP function disrupts the KSHV lytic cycle at early stages post reactivation. To test this hypothesis, we analyzed viral transcriptomes collected by RNAseq of latently infected cells and at 72h post reactivation to determine the impact of BiP inhibition/depletion on viral gene expression at a genome-wide level (Fig 4A–4C and S1 Table). As anticipated, we observed a global reduction in viral transcript levels during the lytic cycle of HA15-treated cells, except for the K2 transcript (encoding vIL6, the viral homolog of interleukin 6) and its overlapping transcript ORF2 (encoding a viral dihydrofolate reductase), both of which increase at 72h post reactivation in HA15-treated cells compared to untreated cells (Fig 4B and 4C and S2 Table) [29,47]. Previous reports have found that XBP1s can bind to the promoter of vIL6 in KSHV-infected cells to induce its expression [48]. Considering that BiP inhibition by HA15 can cause ER stress and UPR activation, we measured the protein levels of XBP1s in a time course of reactivation in the presence of HA15. In these conditions, we could not detect the expression of XBP1s protein in HA15-treated iSLK.219 cells, suggesting that additional factors may compensate for upregulating vIL6 (S5 Fig).

Given the essential role of BiP for folding and processing newly synthesized proteins in the ER, we hypothesized that HA15 treatment could disrupt the lytic cycle by affecting the function of viral glycoproteins expressed during latency or early after reactivation (Table 1). We focused on K1, a KSHV glycoprotein expressed during the latent and lytic cycles of infection, which is required for efficient lytic reactivation [49,50]. Analyses of our RNAseq data revealed

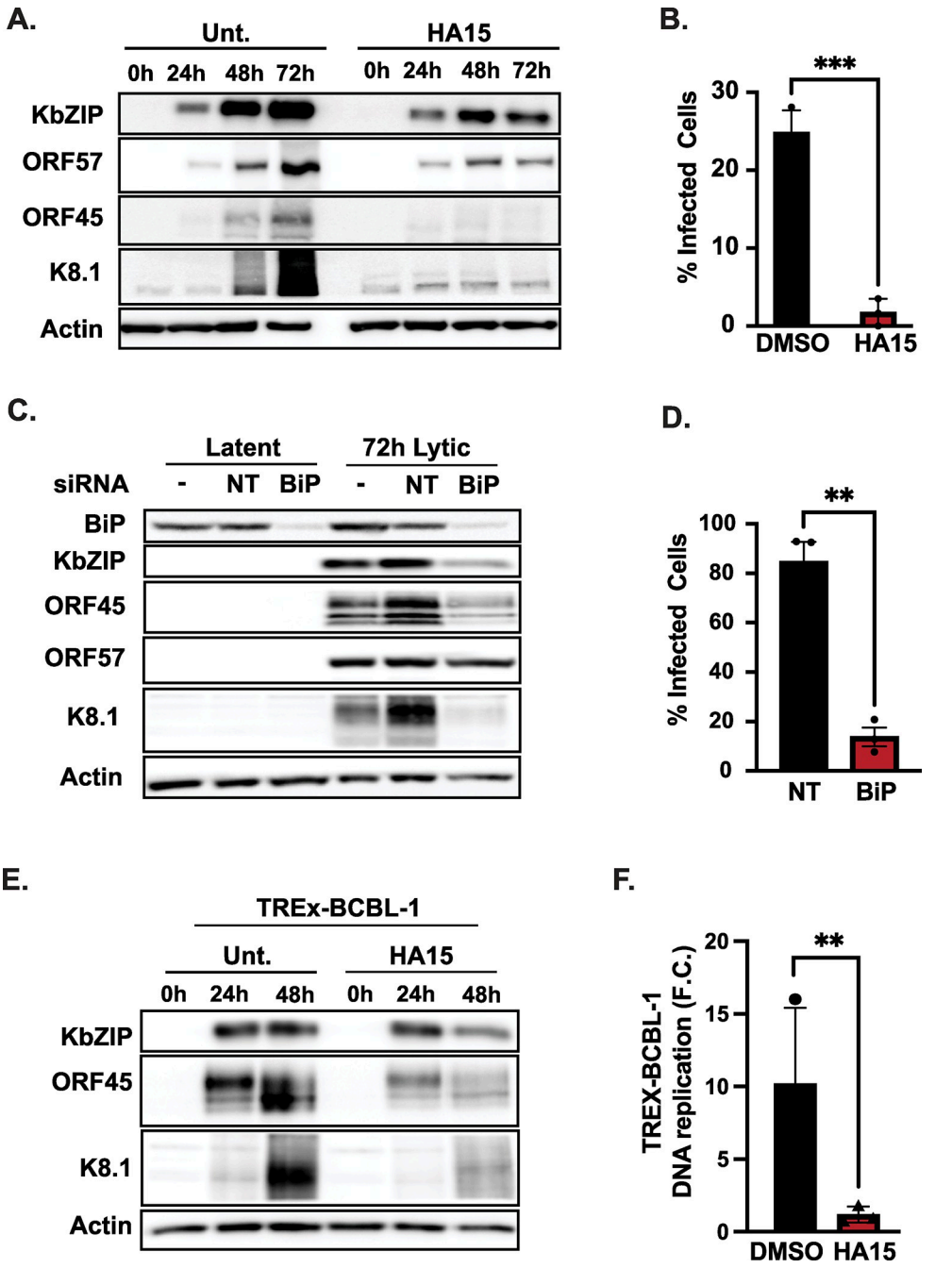

Fig 3. BiP is a pro-viral factor in KSHV-infected cells. (A-B) BiP inhibition with HA15 disrupts the lytic cycle iSLK.219s. **(A)** Cells were treated with HA15 (10 μM) 24h before reactivation with Dox (1 μg/ml). At the indicated times, whole-cell lysates were collected and analyzed by immunoblot for viral proteins (Immediate early: KbZip-nuclear, ORF57-nuclear, Early: ORF45-nuclear/cytosolic, Late: K8.1-glycoprotein). Actin: loading control. **(B)** Supernatants from iSLK.219 cells treated with HA15 were collected at 72h post reactivation and used to infect naïve iSLK cells. GFP expression was determined by automated cell counting at 48h post-infection and used as a proxy for virus production. **(C-D)** Silencing of BiP reduces viral reactivation and infectious virion production. **(C)** iSLK.219 cells were reactivated with Dox, following BiP siRNA-mediated silencing for 48h. Lysates were collected at 72h post-reactivation and analyzed by immunoblot for viral factors. siRNA–untransfected, NT non-targeting **(D)** Supernatants from BiP-KD cells treated as in (C) were collected and processed as described in (B). **(E-F)** Inhibition of BiP blocks the lytic cycle in TREx-BCBL-1-RTA cells. **(E)** Cells were treated with HA15 (10 μM) for 24h before induction with Dox (1 μg/ml). At 48h post-infection, whole cell lysates were collected and analyzed by immunoblot. Actin: loading control. **(F)** Total DNA was isolated from cells treated as in (E), and viral DNA was quantified by qRT-PCR. *N* = 3 independent

biological replicates. Values in (B, D, F) are average ±SEM. Statistical significance was calculated using a paired t-test (B and D) (*P = 0.01, **P = 0.002) or a two-way ANOVA (F) (** P = 0.0065).

https://doi.org/10.1371/journal.ppat.1012660.g003

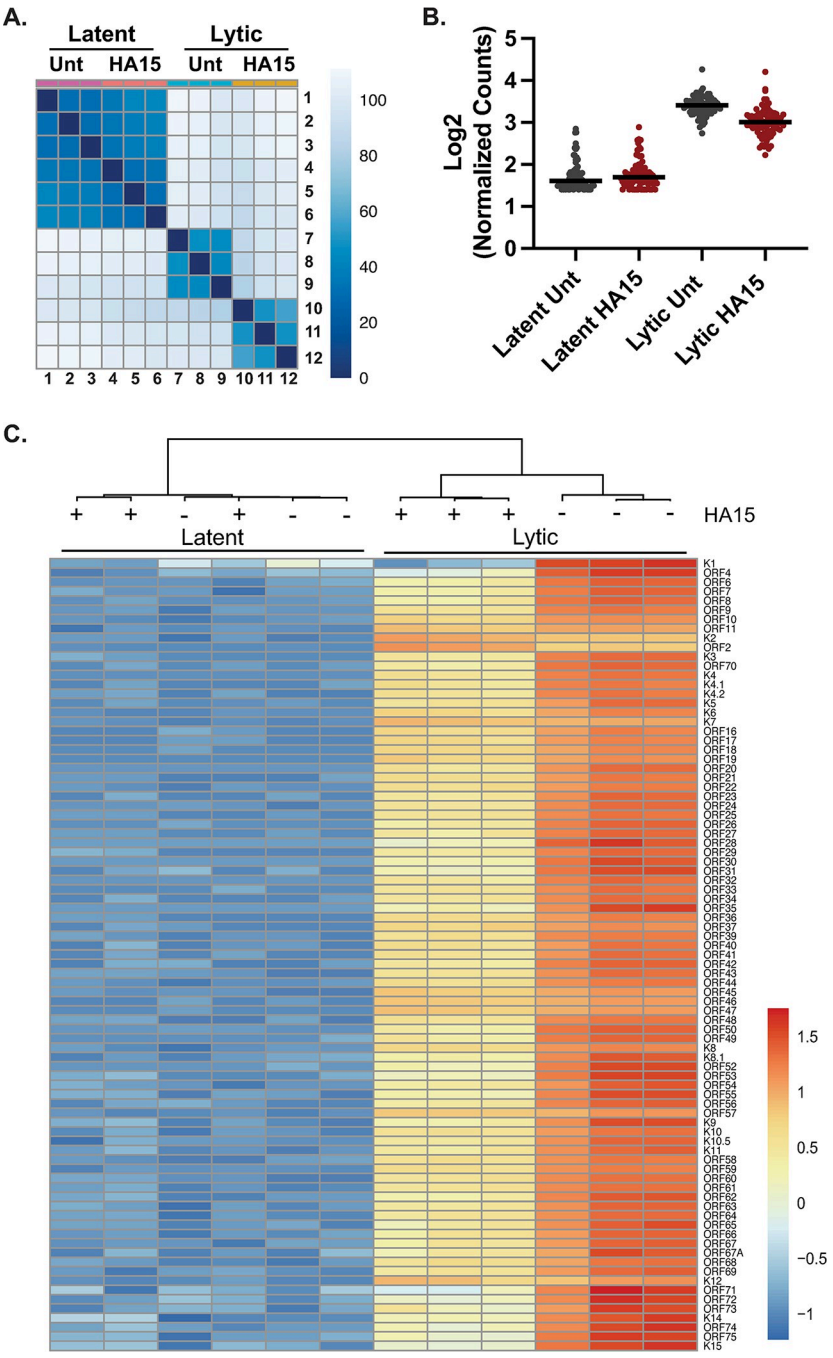

Fig 4. BiP inhibition disrupts the KSHV lytic cycle. **(A-C)** Total RNA was isolated from latent and lytic iSLK.219 cells in the presence or absence of HA15. RNAseq libraries were prepared, sequenced, and aligned to the KSHV genome. **(A)** Pairwise comparison of the RNA-seq samples generated in this study. **(B)** Boxplot of the Log2 of normalized counts of KSHV genes in latent and lytic iSLK.219 cells at 72h post-reactivation in the presence or absence of HA15. **(C)** Heatmap of the scaled normalized counts (Z score) for all KSHV genes ordered by genomic position in lytic iSLK.219 cells ± HA15.

https://doi.org/10.1371/journal.ppat.1012660.g004

the specific downregulation of K1 transcripts in latently infected iSLK.219 cells treated with HA15, and consistently low K1 transcript levels in lytic cells treated with HA15 (Figs 4C and S6A and S2 Table). To assess the impact of HA15 on K1 protein levels, we used TREx-BCBL-1 cells since available antibodies can recognize the K1 protein from PEL cells but not from iSLK.219 cells, due to significant divergence in this gene between isolates. In TREx-BCBL-1-RTA cells, we observed an increase in the levels of K1 as the lytic cycle progressed, in agreement with previous findings [50] (S6B Fig). We see that the levels of K1 are generally lower in latent and lytic cells treated with HA15 (S6A and S6B Fig, S3 Table). The lower levels of K1 in latent iSLK.219 and TREx-BCBL-1 cells may negatively impact the progress of the lytic cycle, thus suggesting that BiP inhibition could disrupt the KSHV lytic cycle at least in part by modulating K1 levels.

Treatment with HA15 is cytostatic for KSHV-infected lymphoma-derived B-cells

In addition to its antiviral activity, HA15 has shown promising anticancer activity [45,51]. To test whether this compound has a similar anticancer effect in KSHV-related lymphomas, we evaluated the impact of escalating doses of HA15 on the viability of three cell lines derived from primary effusion lymphoma, TREx-BCBL-1-RTA, and the BC-1 and BC-2 cell lines that are co-infected with KSHV and EBV (Epstein Barr Virus) (Figs 5A and 5B, S7A-S7D). At 72h post-treatment, we observed a dose-dependent reduction in cell numbers for these cancer cell lines. Even as the total cell numbers were lower in HA15 treatment, the viability of treated cells remained essentially unchanged in all three cell lines at HA15 concentrations $\leq$10 μM. The highest HA15 concentration we tested (50μM) resulted in profound cell cytotoxicity measured by trypan blue exclusion (Figs 5A and 5B and S7A–S7D). These observations suggest HA15 (1–10μM) has a strong cytostatic effect in B-cells derived from primary effusion lymphoma and is cytotoxic to cancer cells at high concentrations. Finally, to test whether these HA15 effects are specific to cancer cells, we treated non-transformed normal peripheral primary B cells (PPBCs) with increasing doses of HA15. These experiments revealed no significant changes in the total number of viable cells compared to untreated cells, even at the highest concentration tested (50μM), indicating that HA15 is neither cytostatic nor cytotoxic for normal B-cells (Fig 5C and 5D).

Treatment with HA15 is cytotoxic for KSHV-infected primary lymphatic endothelial cells

The main cellular targets of KSHV in KS lesions are spindle cells thought to originate from lymphatic endothelial cells (LECs) [52,53]. We used primary LECs as a model for KSHV infection to study the effects of BiP inhibition in a context relevant to the pathophysiology of KS. In this model, we infected LECs with the recombinant KSHV.219 virus, which harbors a puromycin resistance cassette, a constitutive GFP reporter, and an RTA inducible RFP reporter [33,54]. At 14 days post-infection and following puromycin selection (started 48h after infection), KSHV-infected LECs (KLECs.219) expressed GFP and showed the typical spindle cell morphology that is characteristic of KS lesions, corroborating KSHV infection (Fig 5G top middle and left panels). As previously reported, a small fraction of KLECs.219 expressed RFP, indicating spontaneous lytic reactivation in cell culture [54]. In line with our findings in iSLK.219 cells, we observed the upregulation of BiP in KLECs.219 at 14 days post-infection, possibly driven by the expression of lytic genes in a subset of the population (Fig 5E). Treatment of uninfected LECs with 10 μM HA15 for up to 72 h did not substantially affect cell morphology or viability (Fig 5F and 5G). Remarkably and in stark contrast to uninfected LECs,

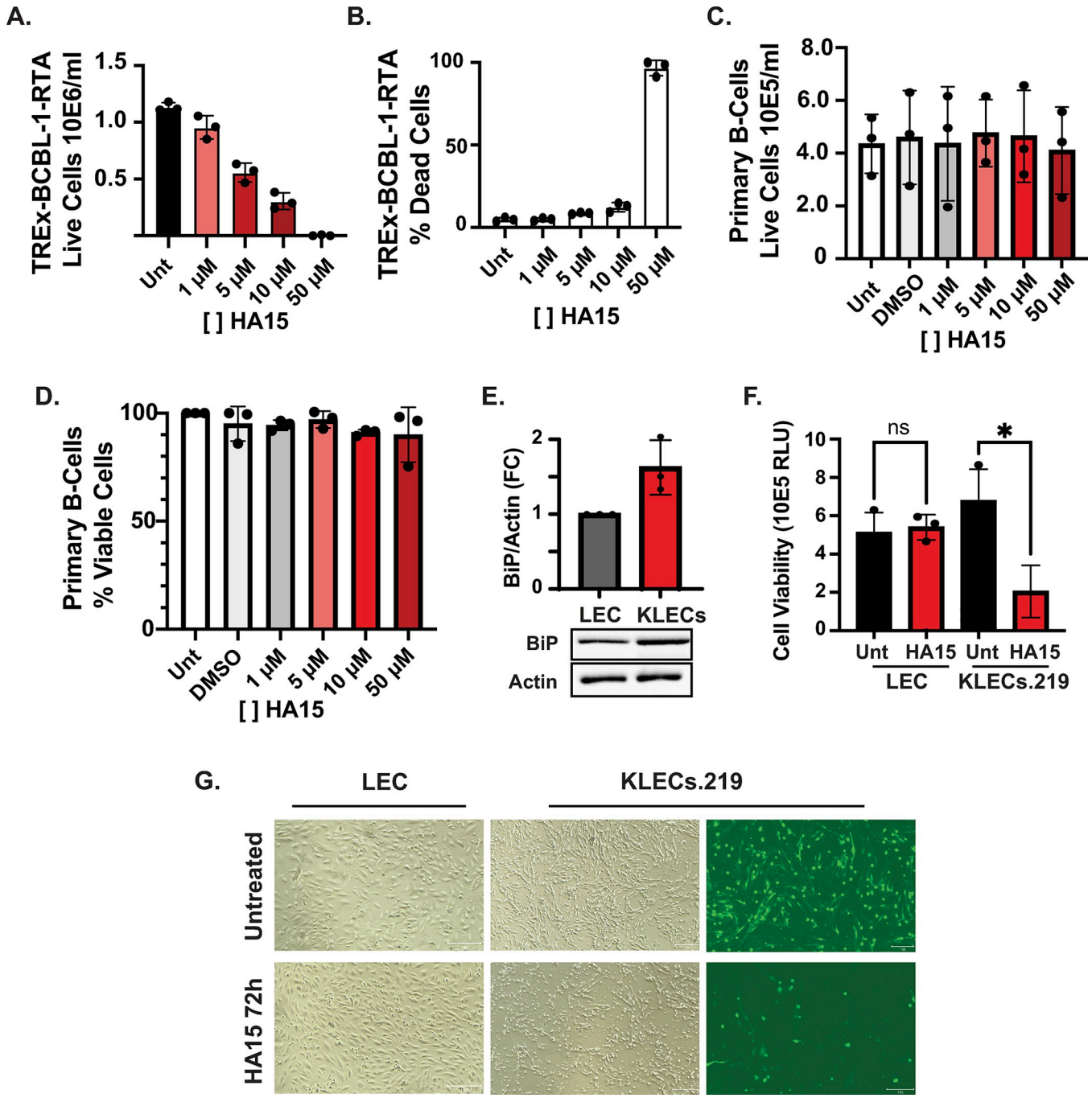

Fig 5. HA15 causes strong cytostasis in latent PEL-derived cells and cytotoxicity in KSHV-infected LEC. (A-B) HA15 treatment differentially reduces cell numbers compared to cell viability in TREx-BCBL-1 cells. Latent TREx-BCBL-1 cells were treated with increasing concentrations of HA15 (0–50 μM) for 72h. The total number of viable cells **(A)** and the percent of dead TREx-BCBL-1 cells **(B)** were determined by automated cell counting following trypan blue staining. **(C-D)** HA15 treatment does not cause cytostasis nor cytotoxicity in primary B cells. Primary Peripheral B-cells were treated with increasing concentrations of HA15 (0–50 μM) for 72h. The total number of viable cells **(C)** and the percent of live cells **(D)** were determined as described in (A-B). $N = 3$ independent biological replicates. Values are average ±SEM. **(E-G)** Primary Lymphatic endothelial cells were infected with KSHV.219 and selected with puromycin for 7–14 days. **(A)** Whole-cell lysates from uninfected (LEC) or infected (KLECs) were collected and analyzed by immunoblot. Actin: loading control. **(B-C)** LECs and KLECs were treated with HA15 (10 μM) for 72h. Cell viability was evaluated by ATP quantification using CellTiter-Glo **(B)** and microscopy at 0h and 72h post-treatment **(C.)**.

https://doi.org/10.1371/journal.ppat.1012660.g005

treating KLECs.219 with 10μM HA15 for 72h induced significant cell death (Fig 5F and 5G), with evident cytotoxicity as early as 48h post-treatment.

HA15 is a broad-spectrum inhibitor of herpes- and poxvirus replication

BiP inhibition with HA15 has been shown as a potential antiviral strategy for RNA viruses, including alphaviruses and, more recently, coronaviruses [19,55]. Our results indicate that this compound is also active against KSHV. Moreover, the upregulation of BiP during infection has also been reported in cells infected by alpha and betaherpesviruses [56,57]. These observations raised the possibility that HA15 may provide antiviral utility against other dsDNA viruses. To test this hypothesis, we evaluated the potential of HA15 to inhibit viral replication in primary human fibroblasts (NHDFs) infected with three different dsDNA viruses: an alphaherpesvirus, Herpes Simplex Virus-1 (HSV-1), a betaherpesvirus, Human Cytomegalovirus (HCMV), and a poxvirus, Vaccinia Virus (VV). Cells were infected at a low multiplicity of infection (MOI) in the presence or absence of HA15. The spread of infection at different times post-infection was determined by measuring the expression of virus-encoded GFP in HSV-1-GFP and HCMV-GFP infected cells or by immunofluorescence using a polyclonal antibody against vaccinia virus [58–60]. Our experiments revealed potent inhibition of viral spread for HSV-1-GFP, HCMV-GFP, and VV in the presence of 10–30 μM HA15, indicating that HA15 acts as a broad-spectrum inhibitor of dsDNA viruses (Fig 6A and 6B). Notably, HA15 treatment of NHDFs was not cytotoxic even at high concentrations (30 μM) or long treatment times (1 or 6 days) (Fig 6C), further substantiating that blocking BiP is a promising antiviral strategy with a minimal negative impact on normal cells.

Discussion

BiP is a pivotal component of the proteostasis network and a pro-viral factor; therefore, it emerges as a potential target for antiviral intervention. Our study uncovered the dysregulation and requirement for BiP during lytic infection by the oncogenic herpesvirus KSHV. Furthermore, we showed that the BiP inhibitor HA15 had a broad-spectrum antiviral activity for dsDNA viruses (herpesviruses and poxviruses) and caused cytostasis/cytotoxicity in KSHV-infected PEL and LEC cells, highlighting its potential use as an anticancer agent during viral-induced oncogenesis.

The cellular response to ER proteostatic insults is orchestrated by the UPR, wherein BiP upregulation is mainly transcriptionally driven by the UPR transcription factors XBP1s and ATF6 [61]. In KSHV-infected iSLK.219 cells, BiP escaped UPR regulatory control and was upregulated post-transcriptionally during lytic infection. Viral infections, including KSHV, induce the integrated stress response (ISR), which has, as a principal outcome, the downregulation of global protein synthesis [62]. In these conditions, cap-dependent translation is disfavored. Thus, the enhanced BiP protein synthesis we observed may arise from alternative initiation mechanisms such as the one afforded by the IRES element in the BiP mRNA [63,64]. Indeed, several stresses negatively impact cap-dependent translation to favor the expression of IRES-containing transcripts [65]. Interestingly, the silencing of the translation initiation factor eIF2A, a distinct protein not to be confused with the widely known eIF2a translation initiation factor, in iSLK.219 cells promoted BiP expression in latent and lytic cells. This finding aligns with previous reports suggesting that eIF2A may suppress IRES-mediated translation in yeast cells and mammalian in vitro translation systems, supporting the notion that the BiP IRES is important for its post-transcriptional regulation [66]. Whether IRES-mediated translation initiation promotes BiP protein upregulation in our system awaits further investigation. Nonetheless, the enhanced translation of upstream open reading frames and non-canonical start

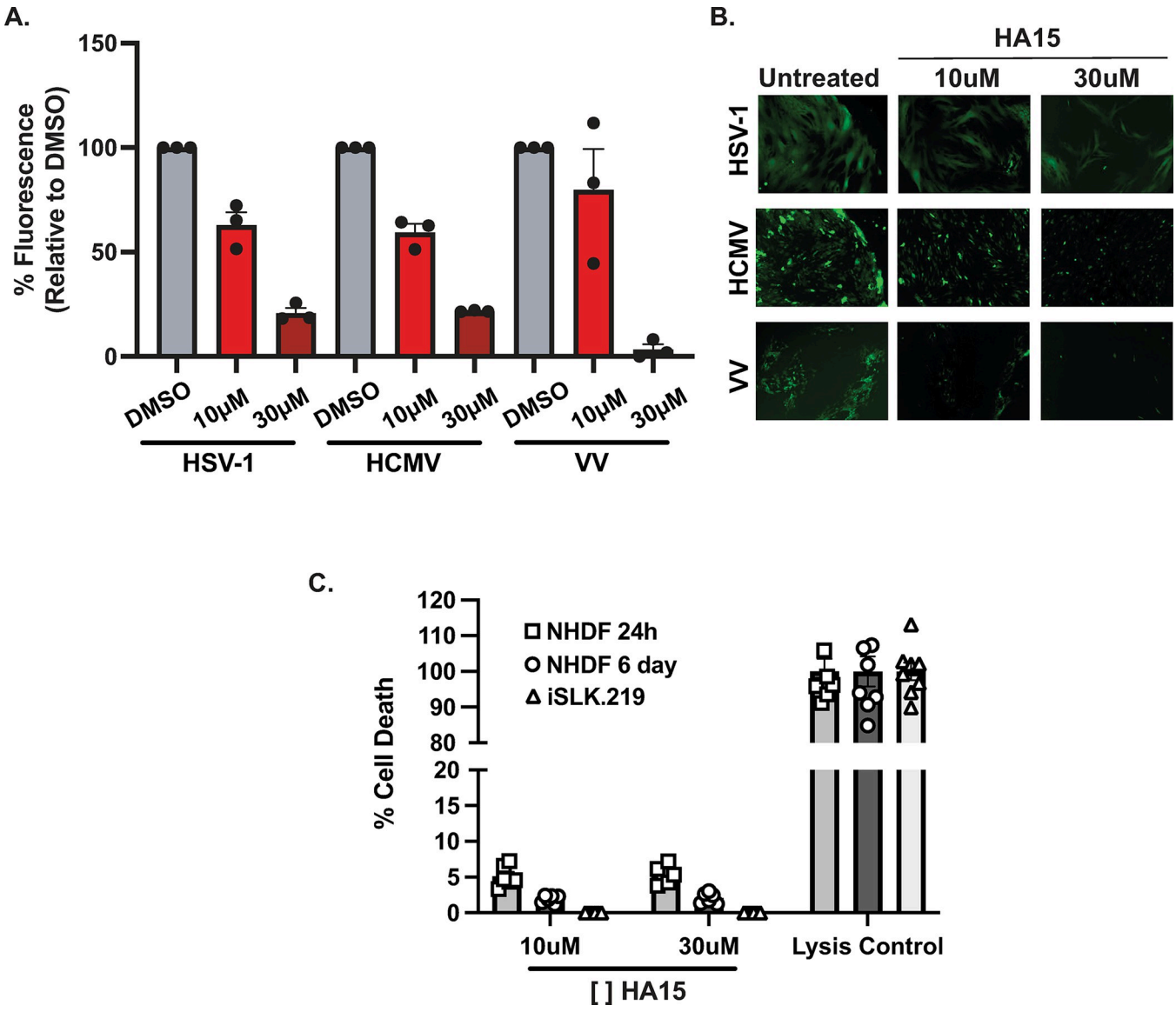

Fig 6. The BiP inhibitor HA15 has a broad-spectrum antiviral effect on herpesviruses and poxviruses. (A-B) Primary human fibroblasts (NHDF) were Infected at a low multiplicity of infection (MOI; HSV-1 at MOI 0.001, HCMV at MOI 0.1, and VV at MOI 0.01) in the presence or absence of HA15 (10 μM or 30 μM). **(A)** The spread of infection was determined at different times post-infection by measuring the expression of virus-encoded GFP in HSV-1-GFP and HCMV-GFP infected cells or by immunofluorescence using a polyclonal antibody against Vaccinia virus. **(B)** Representative images of the samples measured in (A). **(C)** The effect of HA15 treatment on the viability of NDHF (1 or 6 days) and iSLK.219s (3 days) was evaluated by measuring LDH release. N = 3 (A), N = 6 (B) independent biological replicates. Values are average ±SEM.

https://doi.org/10.1371/journal.ppat.1012660.g006

codons reported during the KSHV lytic cycle suggests an altered translational state that could account for the molecular phenotypes we observed [29].

The upregulation of BiP and its pro-viral activity extend beyond KSHV-inherent biology. Indeed, both BiP upregulation and pro-viral roles have been reported in corona-, flavi-, alpha-herpes-, and betaherpesviruses [11,19,55–57]. All these viruses are enveloped; therefore, they rely on the host's machinery to acquire membranes and synthesize and correctly fold viral glycoproteins or secreted viral peptides [2]. In all the viruses mentioned above, BiP has been shown to participate in several steps in the viral cycle, attesting to its essential role in aiding the correct biosynthesis and assembly of proteins during virion production.

In cells infected with the alphavirus VEEV, the flaviviruses DENV or JEV, and the herpesvirus HCMV, genetically or pharmacologically blocking BiP does not impact viral genome replication but significantly reduces infectious virion production [11,55,57]. In these cases, BiP may not be required for the early stages of the viral life cycle but for virion assembly. However, unlike the above observations on HCMV, VEEV, DENV, and JEV-infected cells, in KSHV-infected iSLK.219 and TREx-BCBL-1 cells, BiP inhibition results in a blockage of infection at early stages during reactivation of the lytic cycle before genome replication. The early disruption of the lytic cycle may be partly attributed to the lower levels of the latent and early-lytic glycoprotein K1 we observe in HA15 treated cells. Research from the Damania Lab confirmed that K1 is crucial for efficient KSHV replication [50]. Our experiments consistently show lower levels K1 in lytic TREx-BCBL-1 cells, and reduced levels of the K1 transcript in iSLK.219 cells, both treated with HA15. The downregulation of the K1 proteins in TREX-BCBL-1 cells aligns with an anticipated reduction of ER-folding capacity following BiP-inhibition. On the other hand, the lower levels of K1 transcript may reflect the activation of IRE1-dependent RNA Decay (RIDD), a process by which IRE1 depletes ER-targeted mRNAs upon ER-stress [67]. The K1 transcript, which encodes a peptide with a signal sequence and thus is ER-targeted (Table 1), lacks the conserved endomotif UG|C within a stem loop recognized by IRE1 for cleavage [68]. However, recent reports indicate that IRE1 can cleave mRNAs in an endomotif-independent manner through a process recently coined as RIDDLE (RIDD lacking endomotif). Future research on RIDDLE in KSHV-infected cells will help determine the specificity and dynamics of this process in latent and lytic cells undergoing ER stress. Regardless of the downregulation mechanism, the lower levels of K1 we observed following HA15 treatment, could reduce reactivation, leading to the global downregulation of viral gene expression. Whether additional early-lytic proteins or host factors contribute to the downregulation of lytic reactivation in cells where BiP is no longer active remains to be determined.

While BiP was required for the efficient replication of KSHV in iSLK.219 epithelial cells and PEL-derived TREx-BCBL-1 cells, we noted that the levels of BiP did not increase in PEL-derived cells during the lytic cycle. The virus strains present in these cell lines (iSLK.219 Accession number GQ994935.1 and TREx-BCBL-1 Accession number HQ404500.1) are greater than 99% similar at the nucleotide sequence level, suggesting that the disparate responses we observed likely stem from cell-intrinsic factors. PEL-derived cells show a gene expression profile resembling malignant plasma cells, including a higher expression of the UPR effector XBP1s, and, indeed, higher levels of XBP1s have been observed during the KSHV lytic cycle in TREx-BCBL-1 cells than those observed in iSLK.219 cells [40,69]. The unique gene expression profile of PEL-derived cells may indicate profound reconfiguration of the machinery required for maintaining ER homeostasis in cells with a high secretory burden, as occurs in plasma cells [69, 70]. As such, in TREx-BCBL-1 cells the capacity of the ER may be sufficient to accommodate KSHV protein folding during the lytic cycle without a need to induce signal transduction programs to increase BiP levels. Future studies comparing the basal levels of BiP and other UPR factors in KSHV-infected B- and epithelial cells, as well as the identity and dynamics of BiP client proteins during the viral lytic cycle, will shed light on the inherent ER-protein folding capacity of different KSHV-infected cell types.

Our observations align with the cytoprotective role of BiP, particularly under stress conditions. In line with a maladaptive dependency on BiP in cancer cells, blocking BiP in KSHV-infected PEL and LEC-derived cells resulted in cytostatic and cytotoxic responses, respectively. Indeed, BiP levels are associated with cell division and increased proliferation rates in numerous tumor models [22,71]. One mechanism by which BiP may confer a maladaptive survival advantage is through modulation of cell proliferation by tuning Wnt/B-catenin signaling, wherein BiP-Wnt interactions promote Wnt's correct posttranslational processing to promote

downstream signaling [72]. In PEL cells, the Wnt/B-catenin signaling pathway is usurped by KSHV, and the latency-associated nuclear antigen (LANA), expressed in all KSHV-latently infected cells, arrests GSK3 in the nucleus and promotes the stabilization and accumulation of B-catenin, enabling the entry of infected cells into S-phase [73]. Future experiments to evaluate the integrity of the Wnt/B-catenin signaling pathway in HA15-treated PEL cells will help clarify the contributions of BiP to changes in the proliferation capacity of these lymphoma-derived cells.

In contrast to PEL-derived cells, viral infection in KLECs.219 cells led to the upregulation of BiP and the strict dependence on BiP for cell survival. In other cancers, BiP inhibition leads to a hyperactive UPR, activating apoptosis and autophagy. Detailed mapping of host gene expression and proteome profiles following KSHV infection of LECs and treatment with HA15 will help determine which factors induced upon infection drive terminal responses in KLECs.219 cells.

One of the most exciting observations from our studies is the broad-spectrum antiviral activity of HA15 against both herpes- and poxviruses. Our results substantiate the potential therapeutic application of inhibiting BiP in cells infected by enveloped viruses from unrelated families. A primary concern when targeting host factors for therapeutic antiviral intervention is the potential for cytotoxicity. This concern is paramount when targeting BiP, which is critical for overall cell homeostasis [13,39]. However, our results support the notion that BiP inhibition might be tolerable—we observed minimal cytotoxicity in three primary uninfected cell lines, including peripheral B-cells, lymphatic endothelial cells, and normal human dermal fibroblasts, at concentrations higher than those used to block viral replication. Moreover, *in vivo* studies have shown that BiP haploinsufficiency in aged mice had no significant adverse effects on body weight, organ integrity, behavior, memory, cancer, inflammation, or chemotoxic response [74]. These observations and our results suggest that inhibiting BiP offers a promising therapeutic window for deploying broad-spectrum antivirals.

Materials and methods

Cell culture and compounds

iSLK, iSLK.219, and normal human dermal fibroblasts (NHDFs/Lonza CC-2509) were grown in Dulbecco's modified Eagle medium (DMEM; Invitrogen, Carlsbad, CA, USA) supplemented with 10% FBS, 200 μM of L-glutamine, and 100 U/mL of penicillin and streptomycin. iSLK.219 cells were maintained in 10 μg/mL of puromycin (Invivogen, San Diego, CA, USA). The Primary Effusion Lymphoma (PEL)-derived cells TREx-BCBL1-RTA (Jung Lab Lerner Research Institute at Cleveland Clinic), BC1 (CVCL_1079), and BC2 (CVCL_1856) (Manzano Lab, University of Arkansas for Medical Sciences) were grown in RPMI 1640 medium (Invitrogen, Carlsbad, CA, USA) supplemented with 10% fetal bovine serum (FBS; Invitrogen, Carlsbad, CA, USA), 200 μM of L-glutamine, and 100 U/mL of penicillin/streptomycin. Primary Dermal Lymphatic endothelial cells (LECs) from PromoCell (C-12217) were maintained in EBM-2 media (Lonza 00190860) supplemented with the EGM-2 MV bullet kit (CC-4147) at 37˚C with a 5% CO2 atmosphere. Primary Peripheral B Cells (PPBSc, STEMCELL 70023) were thawed and maintained at 100,000 cells/mL in ImmunoCult™ Human B Cell Expansion media (STEMCELL 100–0645) at 37 degrees Celsius in 5% CO2. Cells were allowed to grow for 7–10 days before treatment with HA15.

The following drugs were used at the concentrations noted; Thapsigargin (Tg) (Tocris 1138) 100nM, Ceapin A7 (Sigma Aldrich SML2330) 6μM, HA15 (Selleckchem S8299) 1–50μM.

Induction and assessment of KSHV reactivation and replication

Exogenous RTA expression was induced in iSLK.219 and TREx-BCBL-1-RTA cells by treatment with 1 μg/mL of doxycycline (Fisher Scientific, Waltham, MA, USA). To prevent viral DNA replication (Fig 1C), these cells were induced with Dox in the presence of phosphonoformate (PFA) 100μM (Sigma Aldrich P6801). Viral reactivation was evaluated by microscopy detection of the PAN-RFP reporter and immunoblot for viral proteins. To determine the efficiency of KSHV DNA replication, DNA was isolated from BCBL-1-RTA at the indicated times following reactivation using the Dneasy blood and tissue kit following manufacturer guidelines (Qiagen 69581). 20ng of total DNA was used for qPCR using primers for the KSHV gene ORF57: F: 5'GGGTGGTTTGATGAGAAGGACA3'R: 5'CGCTACCAAATATGCCACCT, andHuman Chromosome 11q (accession number AP002002.4) as a normalization control: F: 5'TAACTGGTCTTGACTAGGGTTTCAG3'R: 5'ACCACAACAAAAAGCCTTATAGTGG3'

Viruses

HSV1-US11-GFP (Patton strain) (Mohr lab, NYU School of Medicine) was propagated and titrated in Vero cells. HCMV-TB40/E-GFP (Murphy Lab SUNY) was propagated and titrated in NHDFs. Vaccinia Virus Western Reserve (ATCC VR-1354) was expanded in HeLa cells and titrated in BSC1 cells. KSHV.219 was generated from iSLK.219 cells treated with Dox 1ug/ml for 72h. The supernatant from lytic cells was collected, clarified, and filtered with a 0.45 um syringe filter. The virus was tittered by spinoculation (2000 rpm/2 h/Room temp) of uninfected iSLK in 6 well plates. Cells were incubated for 48 h following infection, trypsinized, and collected for flow cytometry in a Sony SH800 instrument. The percentage of cells expressing eGFP was determined by flow cytometry and used to calculate the number of fluorescence forming units (ffus) in each sample.

Immunoblotting and antibodies

Cells were washed and collected in 1X sample buffer (62.5 mM Tris-HCl (pH 6.8), 2% sodium dodecyl sulfate (SDS), 10% glycerol, 0.7 M b-mercaptoethanol). Samples were sonicated on ice to reduce viscosity. Cell lysates were fractionated by SDS-PAGE and transferred onto nitrocellulose membranes. Immunoblots were incubated with primary antibodies overnight at 4˚C, and immunoreactive bands were detected with HRP-conjugated secondary antibodies by enhanced chemiluminescence (ThermoFisher, Waltham, MA, USA) according to the manufacturer's recommendations. All antibodies were used at a 1:1000 dilution in 3% BSA/1× TBST unless indicated. BiP (Cell Signaling Technologies 3117), Actin (1:30,000, Sigma Aldrich, St. Louis, MO, USA), GRP94 (Cell Signaling Technologies 2104), Calreticulin (Cell Signaling Technologies 2891, IRE1 (Cell Signaling Technologies 3294), IRE1-P Ser274 (Novus biotechnologies NB100-2323), XBP1s (Cell Signaling Technologies 40435), K8.1 (mAb clone 19B4), vIL6 (Advanced Biotechnology 13-214-050), KbZip (SCBT sc-69797), ORF45 (SCBT sc-53883), ORF57 (SBCT sc-135746). The LANA rabbit polyclonal antibody was raised against a synthetic peptide from the acidic domain of LANA (Polson and Ganem). The antibody for K1 (1:100) was a generous gift from the Damania Lab at The University of North Carolina at Chapel Hill.

CRISPRi-mediated knockdown

Synthetic DNA segments encoding the sgRNAs targeting ATF6 (5'GTTAATATCTGGGACGGCGG3') or XBP1 (5'GCCGCCACGCTGGGAACCTA3') were cloned into the BlpI and BstXI restriction sites in the pLG15 (CRISPRi) vector. The positive clones were confirmed

by Sanger sequencing. Vesicular stomatitis virus (VSV) pseudotyped lentiviral production followed standard protocols. Briefly, 293METR packaging cell lines were transfected with the pLG15 lentiviral vector, VSV-G plasmid (pMD2.G Addgene 12259), and pCMV delta R8.2 (Addgene 12263). At 48h post-transfection, the viral supernatant was collected, clarified by centrifugation, and filtered through a 0.45 μm filter to remove cell debris. Viral particles were concentrated 5-fold using a regenerated cellulose centrifugal filter unit with a 100k MW cut-off (Amicon Ultracel 100k). The resulting lentivirus stock was used to transduce iSLK.219-d-Cas9-KRAB cells by spinoculation [41]. Transduced iSLK.219 cells were maintained in 10 μg/mL of puromycin and were selected for BFP+/sgRNA+ expression by FACS in a Sony SH800 instrument. Knockdown of ATF6 and XBP1s was confirmed by qPCR or immunoblot, respectively.

Reverse Transcription PCR (RT-PCR) and Quantitative PCR (qPCR)

Total cellular and viral RNA was isolated from cells using the RNAeasy Plus Mini kit (QIAGEN 74134) following manufacturers' recommendations. Reverse-transcription (RT)-PCR was performed using 500–1000 ng of total RNA per RT reaction using the iScript Reverse Transcription Supermix. To remove excess genomic DNA, samples were treated with Dnase (New England Biolabs Inc. M0303). PCR was done using 1% of the resulting cDNA as a template. For the detection of XBP1-s and XBP1-u mRNAs, we used the following primer pairs: XBP1u/s: F: 5'GGAGTTAAGACAGCGCTTGG3'R: 5'ACTGGGTCCAAGTTGTCCAG3'. Products were separated on a 3% agarose gel and quantified by scanning densitometry (ImageJ). BiP mRNA abundance changes were measured by real-time RT-PCR analysis using the PowerUp SYBR Green Master Mix. All qPCR reactions were done in a C1000 Touch Thermal cycler with a CFX96 Real-Time System. Samples were normalized using 28S RNA. Primers: 28S: F: 5'AAACTCTGGTGGAGGTCCGT3'R: 5'CTTACCAAAAGTGGCCCACTA3', BiP (HSPA5): F: 5'AGTTCCAGCGTCTTTGGTTG3'R: 5'TGCAGCAGGACATCAAGTTC3'

Total cellular and viral DNA was isolated from iSLK cells infected with KSHV.219 at 72h post-infection using the Zymo Research Quick-DNA Miniprep Plus (Zymo D4068). The levels of viral DNA were determined by quantitative PCR analysis using the Luna Universal qPCR MasterMix (NEB M3003). Viral genome levels were normalized to GAPDH to account for loading differences. LANA: F: 5'TCCAAAGTGTCAATGGAAGT3'R: 5'GTAGATGGGTC GTGAGAACA3', GAPDH: F: 5'AAGGGCCCTGACAACTCTTTT3'R: 5'CTGGTGGTCCA GGGGTCTTA3'

siRNA-mediated knockdown

Small interfering RNAs targeting BiP (NM_005347) were ordered as a SMARTpool from Dharmacon (ON-TARGETplus Human HSPA5 siRNA L-008198-00-0005). The ON-TARGETplus Non-targeting Control Pool was used as a negative control (D-001810-10-05). iSLK.219 cells (2x10e5 cells/well) were transfected with 100nM of the siRNA mix using DharmaFect transfection reagent. At 24h post-silencing, cells were treated with 1 μg/mL Dox to induce viral lytic reactivation. BiP silencing was confirmed by immunoblot. For eIF2A silencing, single siRNAs were ordered from Santa Cruz Biotechnologies (eIF2A-siRNA sc-78713, Non-targeting-siRNA sc-37007). Cells were transfected using Lipofectamine RNAiMax transfection reagent following manufacturers recommendations (Invitrogen 13778075). At 48h post-silencing, cells were treated with 1 μg/mL Dox to induce viral lytic reactivation. eIF2A silencing was confirmed by immunoblot.

RNA sequencing and analysis

Total cellular and viral RNA was isolated from iSLK.219 cells at 72h post reactivation in the presence or absence of 10μM HA15, using the RNAeasy Plus Mini kit (QIAGEN 74134) following manufacturers' recommendations, including a DNAse treatment step. RNA sequencing libraries were generated using the NEBNext Ultra II RNA Library Prep Kit (New England BioLabs E7760) and sequenced using a 150bp paired-end protocol on an Illumina NextSeq 550 instrument. Following demultiplexing, the sequenced reads were aligned to the human genome GRcHg38 version 41 and the KSHV genome GQ994935.1. Read abundance and differential gene expression were determined using the DESeq2 package. RNA-seq data and the code used in this study were uploaded to the GEO database with the accession number GSE 280006.

Fluorescence assay

Primary normal human dermal (NHDF) cells were plated at a density of 30,000 cells per well in a 96-well plate. The following day, cells were pretreated for two hours with HA15 (DMSO final concentration 0.1%) and incubated at 37˚C. After pretreatment, NHDF cells were either mock-infected or infected with Herpes simplex virus 1 (HSV-1) US11-GFP (Patton strain) at MOI 0.01, Human cytomegalovirus (HCMV) EGFP (TB40/E strain) at MOI 0.1, or Vaccinia virus (VV) (Western Reserve strain) at MOI 0.1 and incubated for 1h at 37˚C. After 1h incubation, the supernatant from cells was removed and replaced with fresh DMEM and HA15. Cells were incubated at 37˚C for 24 h (HSV-1 and VV-infected cells) or 6 days (HCMV-infected cells). After respective incubation periods, the supernatant was removed and replaced with PBS. Because VV lacked a fluorescent reporter, infected cells were stained with primary antibody (Vaccinia Virus Polyclonal FITC Antibody ThermoFisher PA1-73191, 1:1000) and Hoechst 33342 (1:10,000). The fluorescent signal (GFP/Hoescht) was analyzed using the SpectraMax i3x plate reader. GFP fluorescence was measured at 485/535 and Hoescht fluorescence at 350/461.

Cell viability assays

TREx-BCBL1-RTA, BC1, and BC2 cells were seeded at a density of 30,000 cells per well in a 96-well plate. The following day, cells were treated with increasing doses of HA15 (1μM, 5μM, 10μM, and 50μM). At 72 hours post-treatment, 10μl of the cells were stained with trypan blue and counted using the countess automated cell counter (ThermoFisher) to determine the number of live cells/ml and the percent cell death.

LEC viability was determined using the CellTiter-Glo Luminescent Cell Viability Assay (Promega). Uninfected and KSHV-infected LECs were seeded at a density of 7,500–10,000 cells per well of a white 96-well plate. The following day, cells were treated with HA15 (10 μM). At 72h post-treatment, the media was replaced, and an equal volume of the CellTiter-Glo reagent was added to each well. The plate was incubated in the dark for 10–15 minutes before luminescence was read on a Victor^{3}V 1420 Multilabel Counter (Perkin Elmer).

Primary normal human dermal (NHDF) cells were plated at a density of 30,000 cells per well in a 96-well plate. The following day, cells were treated with HA15 (DMSO final concentration 0.1%) and incubated at 37˚C. At 24h or 6 days (corresponding to the viral infection period), 50 μL of supernatant was transferred to a new 96-well plate. 50 μL of CytoTox-ONE reagent was added to the plate and incubated at RT for 10 minutes. After 10 minutes, 25 μL of Stopping Reagent was added to the plate, and the plate was incubated at RT for 10 minutes. After incubation, the plate was transferred to the SpectraMax i3x plate reader, and fluorescence was read at 560/590 to determine percent cytotoxicity.

Supporting information

S1 Fig. KSHV reactivation in iSLK.219 cells follows a cascade of gene expression. Latently infected iSLK.219 cells were induced to enter the lytic cycle by exogenous expression of RTA following Dox (1 μg/ml) treatment. **(A)** Imaging of cells at 72h post reactivation showing the expression of the lytic PAN-RFP marker in the population. **(B)** Immunoblot for viral proteins in iSLK.219 lysates collected at the indicated time points. Images are representative of 3 independent biological replicates. Actin: loading control.
(TIF)

S2 Fig. eIF2A suppresses BiP translation in iSLK.219 cells. iSLK.219 cells were transfected with a non-targeting siRNA, or an siRNA targeting eIF2A (scbt Cat78713). Cells were grown for 3 days prior to treatment with 1ug/ml dox for 48h. (Left) Whole-cell lysates collected at 48h post-dox treatment were analyzed by immunoblot. GAPDH: loading control. (Right) Image densitometry quantification of the BiP immunoblot. N = 3 (eIF2A antibody proteintech 11233-1-AP, BiP antibody C50B12, GAPDH 14C10).
(TIF)

S3 Fig. HA15 does not alter cell viability, the establishment of latency, or the activity of RTA in iSLK cells. Latently infected iSLK.219 cells were induced to enter the lytic cycle by exogenous expression of RTA following Dox (1 μg/ml) treatment for 24h-48h in the presence or absence of HA15 10 μM. **(A)** Cells were collected at 48h, stained with trypan blue, and counted to measure viability. **(B)** Histograms showing the numbers of cells and fluorescence intensity of GFP and RFP measured by flow cytometry analysis. **(C)** Quantification of GFP and RFP positive cells from (B). **(D)** To determine the impact of HA15 on the establishment of latency, uninfected iSLK cells were pre-treated with HA15 for 24h before infection with KSHV.219 at high and low MOIs. Cells were incubated for 72h, and viral genome levels were quantified by qPCR of LANA using total DNA as input. GAPDH amplification was used for normalization. N = 3.
(TIF)

S4 Fig. BiP levels do not increase during the KSHV lytic cycle in TREx-BCBL-1 cells. TREx-BCBL-1 cells were reactivated with Dox (2 μg/ml). At 4h before collection, cells were treated with Tg (100 nM) for 4h to induce acute ER stress. Whole-cell lysates were collected at the indicated times. Actin: loading control.
(TIF)

S5 Fig. HA15 treatment of iSLK.219 does not induce XBP1s expression. Latent iSLK.219 cells were reactivated in the presence or absence of HA15 (10μM). Whole-cell lysates collected at the indicated times were analyzed by immunoblot using an antibody specific for XBP1s. Actin: loading control.
(TIF)

S6 Fig. K1 expression decreases in HA15 treated cells. (A) Log2 fold change of latent transcripts levels in iSLK.219 cells treated with HA15 for 48h vs. untreated. **(B)** HA15 treatment reduces K1 levels during the KSHV lytic cycle. (top) TREx-BCBL-1-RTA cells were treated with HA15 (10 μM) 24h before induction with Dox (1 ug/ml). At 48h post-infection, whole cell lysates were collected and analyzed by immunoblot. Actin: loading control. (bottom) Image quantification by gel densitometry of the K1 immunoblot. *N* = 3 independent biological replicates. Values in (C) are average ±SD.
(TIF)

S7 Fig. HA15 has a cytostatic effect on PEL-derived cells. (A-D) HA15 treatment causes cytostasis in BC-1 and BC-2 cells latently co-infected with KSHV and EBV. Cells were treated with increasing doses of HA15 (0–50 μM) for 72h. The total number of viable **(A)** and the percent of dead BC-1 cells **(B)** were determined by automated cell counting following trypan blue staining. The total number of viable **(C)** and the percent of dead BC-2 cells **(D)** were determined by automated cell counting following trypan blue staining. $N = 3$ independent biological replicates. Values are average ±SEM.
(TIF)

S1 Table. RNAseq raw counts.
(XLSX)

S2 Table. RNAseq Z-scores for KSHV genes.
(XLSX)

S3 Table. RNAseq Log2 Fold change for KSHV genes.
(XLSX)

Acknowledgments

We thank Norma Neff and the CZ BioHub genomics platform for their help with RNA sequencing. We thank Carlos Gutierrez and Anna van Dorsten for their technical help. We are grateful for the support, scientific discussions, and critical proofreading from S. Schmid, A. Kistler, and R. Aviner at CZ BioHub, San Francisco; D. Acosta-Alvear, F. Braig-Karzig, and F. Zappa at Altos Labs; and Z. Aralis and D. Proctor at UCSB.

Author Contributions

Conceptualization: Guillermo Najarro, Carolina Arias.

Data curation: Guillermo Najarro, Leah C. Dorman, Carolina Arias.

Formal analysis: Leah C. Dorman.

Funding acquisition: Carolina Arias.

Investigation: Guillermo Najarro, Kevin Brackett, Hunter Woosley, Vincent Turon-Lagot, Sudip Khadka, Catya Faeldonea, Osvaldo Kevin Moreno, Adriana Ramirez Negron, Christina Love, Ryan Ward, Charles Langelier.

Methodology: Guillermo Najarro, Kevin Brackett, Hunter Woosley, Adriana Ramirez Negron, Christina Love, Ryan Ward, Frank McCarthy, Carlos Gonzalez, Joshua E. Elias, Carolina Arias.

Resources: Joshua E. Elias.

Supervision: Charles Langelier, Joshua E. Elias, Brooke M. Gardner, Carolina Arias.

Visualization: Leah C. Dorman, Vincent Turon-Lagot, Frank McCarthy, Carlos Gonzalez.

Writing – original draft: Guillermo Najarro, Carolina Arias.

Writing – review & editing: Guillermo Najarro, Kevin Brackett, Hunter Woosley, Vincent Turon-Lagot, Sudip Khadka, Osvaldo Kevin Moreno, Charles Langelier, Frank McCarthy, Carlos Gonzalez, Brooke M. Gardner, Carolina Arias.

References

1. Stern-Ginossar N, Thompson SR, Mathews MB, Mohr I. Translational Control in Virus-Infected Cells. Cold Spring Harb Perspect Biol. 2019; 11: a033001. https://doi.org/10.1101/cshperspect.a033001 PMID: 29891561
2. Aviner R, Frydman J. Proteostasis in Viral Infection: Unfolding the Complex Virus-Chaperone Interplay. Cold Spring Harb Perspect Biol. 2020; 12. https://doi.org/10.1101/cshperspect.a034090 PMID: 30858229
3. Paladino L, Vitale AM, Bavisotto CC, de Macario EC, Cappello F, Macario AJL, et al. The role of molecular chaperones in virus infection and implications for understanding and treating covid-19. Journal of Clinical Medicine. MDPI; 2020. pp. 1–15. https://doi.org/10.3390/jcm9113518 PMID: 33143379
4. Zhang X, Yu W. Heat shock proteins and viral infection. Front Immunol. 2022; 13. https://doi.org/10.3389/fimmu.2022.947789 PMID: 35990630
5. Evelyne K, Sébastien C, Valentin B, Laurence D, Natalia B-B, Oleg D, et al. Endoplasmic Reticulum Chaperones in Viral Infection: Therapeutic Perspectives. Microbiology and Molecular Biology Reviews. 2021; 85: e00035–21. https://doi.org/10.1128/MMBR.00035-21 PMID: 34643441
6. Saibil H. Chaperone machines for protein folding, unfolding and disaggregation. Nature Reviews Molecular Cell Biology. 2013. pp. 630–642. https://doi.org/10.1038/nrm3658 PMID: 24026055
7. Hartl FU, Bracher A, Hayer-Hartl M. Molecular chaperones in protein folding and proteostasis. Nature. 2011; 475: 324–332. https://doi.org/10.1038/nature10317 PMID: 21776078
8. Ravindran MS, Bagchi P, Cunningham CN, Tsai B. Opportunistic intruders: How viruses orchestrate ER functions to infect cells. Nature Reviews Microbiology. Nature Publishing Group; 2016. pp. 407–420. https://doi.org/10.1038/nrmicro.2016.60 PMID: 27265768
9. Chen S, Novick P, Ferro-Novick S. ER structure and function. Current Opinion in Cell Biology. 2013. pp. 428–433. https://doi.org/10.1016/j.ceb.2013.02.006 PMID: 23478217
10. Pobre KFR, Poet GJ, Hendershot LM. The endoplasmic reticulum (ER) chaperone BiP is a master regulator of ER functions: Getting by with a little help from ERdj friends. Journal of Biological Chemistry. American Society for Biochemistry and Molecular Biology Inc.; 2019. pp. 2098–2108. https://doi.org/10.1074/jbc.REV118.002804 PMID: 30563838
11. Lewy TG, Grabowski JM, Bloom ME. BiP: Master Regulator of the Unfolded Protein Response and Crucial Factor in Flavivirus Biology. YALE JOURNAL OF BIOLOGY AND MEDICINE. 2017; 90(2):291–300.
12. Kimata Y, Oikawa D, Shimizu Y, Ishiwata-Kimata Y, Kohno K. A role for BiP as an adjustor for the endoplasmic reticulum stress-sensing protein Ire1. Journal of Cell Biology. 2004; 167: 445–456. https://doi.org/10.1083/jcb.200405153 PMID: 15520230
13. Lai CW, Aronson DE, Snapp EL. BiP Availability Distinguishes States of Homeostasis and Stress in the Endoplasmic Reticulum of Living Cells. Mol Biol Cell. 2010; 21: 1909–1921. https://doi.org/10.1091/mbc.e09-12-1066 PMID: 20410136
14. Preissler S, Ron D. Early events in the endoplasmic reticulum unfolded protein response. Cold Spring Harb Perspect Biol. 2019; 11. https://doi.org/10.1101/cshperspect.a033894 PMID: 30396883
15. Walter P, Ron D. The Unfolded Protein Response: From Stress Pathway to Homeostatic Regulation. 2011; 334:6059. https://doi.org/10.1126/science.1209038 PMID: 22116877
16. Karagöz GE, Acosta-Alvear D, Walter P. The Unfolded Protein Response: Detecting and Responding to Fluctuations in the Protein-Folding Capacity of the Endoplasmic Reticulum. Cold Spring Harb Perspect Biol. 2019; 11: a033886. https://doi.org/10.1101/cshperspect.a033886 PMID: 30670466
17. Tan Z, Zhang W, Sun J, Fu Z, Ke X, Zheng C, et al. ZIKV infection activates the IRE1-XBP1 and ATF6 pathways of unfolded protein response in neural cells. J Neuroinflammation. 2018; 15. https://doi.org/10.1186/s12974-018-1311-5 PMID: 30241539
18. Wati S, Soo M-L, Zilm P, Li P, Paton AW, Burrell CJ, et al. Dengue Virus Infection Induces Upregulation of GRP78, Which Acts To Chaperone Viral Antigen Production. J Virol. 2009; 83: 12871–12880. https://doi.org/10.1128/JVI.01419-09 PMID: 19793816
19. Shin WJ, Ha DP, Machida K, Lee AS. The stress-inducible ER chaperone GRP78/BiP is upregulated during SARS-CoV-2 infection and acts as a pro-viral protein. Nature Communications. Nature Research; 2022. https://doi.org/10.1038/s41467-022-34065-3 PMID: 36376289
20. Shu W, Guo Z, Li L, Xiong Z, Wang Z, Yang Y, et al. Regulation of Molecular Chaperone GRP78 by Hepatitis B Virus: Control of Viral Replication and Cell Survival. Mol Cell Biol. 2020;40. https://doi.org/10.1128/MCB.00475-19 PMID: 31712392
21. Buchkovich NJ, Yu Y, Pierciey FJ, Alwine JC. Human Cytomegalovirus Induces the Endoplasmic Reticulum Chaperone BiP through Increased Transcription and Activation of Translation by Using the BiP

Internal Ribosome Entry Site. J Virol. 2010; 84: 11479–11486. https://doi.org/10.1128/JVI.01330-10 PMID: 20739513

22. Lee AS. Glucose-regulated proteins in cancer: molecular mechanisms and therapeutic potential. Nat Rev Cancer. 2014; 14: 263–276. https://doi.org/10.1038/nrc3701 PMID: 24658275
23. Ronco C, Rocchi S, Benhida R. Expression level of GRP78/BiP as a predictor of favorable or unfavorable outcomes in cancer patients. Mediastinum. 2018; 2: 26–26. https://doi.org/10.21037/med.2018.03.18
24. Li T, Fu J, Cheng J, Elfiky AA, Wei C, Fu J. New progresses on cell surface protein HSPA5/BiP/GRP78 in cancers and COVID-19. Front Immunol. 2023; 14. https://doi.org/10.3389/fimmu.2023.1166680 PMID: 37275848
25. Roller C, Maddalo D. The molecular chaperone GRP78/BiP in the development of chemoresistance: Mechanism and possible treatment. Frontiers in Pharmacology. 2013. https://doi.org/10.3389/fphar.2013.00010 PMID: 23403503
26. Gaglia MM. Kaposi's sarcoma-associated herpesvirus at 27. Tumour Virus Research. Elsevier B.V.; 2021. https://doi.org/10.1016/j.tvr.2021.200223 PMID: 34153523
27. Cesarman E, Chadburn A, Rubinstein PG. KSHV/HHV8-mediated hematologic diseases. Blood. 2022; 139: 1013–1025. https://doi.org/10.1182/blood.2020005470 PMID: 34479367
28. Purushothaman P, Dabral P, Gupta N, Sarkar R, Verma SC. KSHV genome replication and maintenance. Frontiers in Microbiology. Frontiers Media S.A.; 2016. https://doi.org/10.3389/fmicb.2016.00054 PMID: 26870016
29. Arias C, Weisburd B, Stern-Ginossar N, Mercier A, Madrid AS, Bellare P, et al. KSHV 2.0: A Comprehensive Annotation of the Kaposi's Sarcoma-Associated Herpesvirus Genome Using Next-Generation Sequencing Reveals Novel Genomic and Functional Features. PLoS Pathog. 2014; 10: e1003847. https://doi.org/10.1371/journal.ppat.1003847 PMID: 24453964
30. Purushothaman P, Uppal T, Verma SC. Molecular biology of KSHV lytic reactivation. Viruses. MDPI AG; 2015. pp. 116–153. https://doi.org/10.3390/v7010116 PMID: 25594835
31. Schlesinger M, McDonald C, Ahuja A, Alvarez Canete CA, Nuñez del Prado Z, Naipauer J, et al. Glucose and mannose analogs inhibit KSHV replication by blocking N-glycosylation and inducing the unfolded protein response. J Med Virol. 2023;95. https://doi.org/10.1002/jmv.28314 PMID: 36380418
32. Myoung J, Ganem D. Generation of a doxycycline-inducible KSHV producer cell line of endothelial origin: Maintenance of tight latency with efficient reactivation upon induction. J Virol Methods. 2011; 174: 12–21. https://doi.org/10.1016/j.jviromet.2011.03.012 PMID: 21419799
33. Vieira J, O'Hearn PM. Use of the red fluorescent protein as a marker of Kaposi's sarcoma-associated herpesvirus lytic gene expression. Virology. 2004; 325: 225–240. https://doi.org/10.1016/j.virol.2004.03.049 PMID: 15246263
34. Kedes DH, Ganem D. Sensitivity of Kaposi's Sarcoma-associated Herpesvirus Replication to Antiviral Drugs Implications for Potential Therapy. J Clin Invest. 1997; 99(9):2082. https://doi.org/10.1172/JCI119380 PMID: 9151779
35. Käll L, Krogh A, Sonnhammer ELL. A Combined Transmembrane Topology and Signal Peptide Prediction Method. J Mol Biol. 2004; 338: 1027–1036. https://doi.org/10.1016/j.jmb.2004.03.016 PMID: 15111065
36. Teufel F, Almagro Armenteros JJ, Johansen AR, Gíslason MH, Pihl SI, Tsirigos KD, et al. SignalP 6.0 predicts all five types of signal peptides using protein language models. Nat Biotechnol. 2022; 40: 1023–1025. https://doi.org/10.1038/s41587-021-01156-3 PMID: 34980915
37. Hiller K, Grote A, Scheer M, Munch R, Jahn D. PrediSi: prediction of signal peptides and their cleavage positions. Nucleic Acids Res. 2004; 32: W375–W379. https://doi.org/10.1093/nar/gkh378 PMID: 15215414
38. Hallgren J, Tsirigos KD, Pedersen MD, Armenteros JJA, Marcatili P, Nielsen H, et al. DeepTMHMM predicts alpha and beta transmembrane proteins using deep neural networks. bioRxiv. 2022; 2022.04.08.487609. https://doi.org/10.1101/2022.04.08.487609
39. Vitale M, Bakunts A, Orsi A, Lari F, Tadè L, et al. Inadequate BiP availability defines endoplasmic reticulum stress. 2019. https://doi.org/10.7554/eLife.41168 PMID: 30869076
40. Johnston BP, Pringle ES, McCormick C. KSHV activates unfolded protein response sensors but suppresses downstream transcriptional responses to support lytic replication. PLoS Pathog. 2019; 15: e1008185. https://doi.org/10.1371/journal.ppat.1008185 PMID: 31790507
41. Brackett K, Mungale A, Lopez-Isidro M, Proctor DA, Najarro G, Arias C. CRISPR Interference Efficiently Silences Latent and Lytic Viral Genes in Kaposi's Sarcoma-Associated Herpesvirus-Infected Cells. Viruses. 2021; 13. https://doi.org/10.3390/v13050783 PMID: 33924938

42. Torres SE, Gallagher CM, Plate L, Gupta M, Liem CR, Guo X, et al. Ceapins block the unfolded protein response sensor ATF6a by inducing a neomorphic inter-organelle tether. 2019. https://doi.org/10.7554/eLife.46595.001

43. Starck SR, Tsai JC, Chen K, Shodiya M, Wang L, Yahiro K, et al. Translation from the 5′ untranslated region shapes the integrated stress response. Science (1979). 2016; 351. https://doi.org/10.1126/science.aad3867 PMID: 26823435

44. Glaunsinger B, Chavez L, Ganem D. The Exonuclease and Host Shutoff Functions of the SOX Protein of Kaposi's Sarcoma-Associated Herpesvirus Are Genetically Separable. J Virol. 2005; 79: 7396–7401. https://doi.org/10.1128/JVI.79.12.7396-7401.2005 PMID: 15919895

45. Cerezo M, Lehraiki A, Millet A, Rouaud F, Plaisant M, Jaune E, et al. Compounds Triggering ER Stress Exert Anti-Melanoma Effects and Overcome BRAF Inhibitor Resistance. Cancer Cell. 2016; 29: 805–819. https://doi.org/10.1016/j.ccell.2016.04.013 PMID: 27238082

46. Nakamura H, Lu M, Gwack Y, Souvlis J, Zeichner SL, Jung JU. Global Changes in Kaposi's Sarcoma-Associated Virus Gene Expression Patterns following Expression of a Tetracycline-Inducible Rta Transactivator. J Virol. 2003; 77: 4205–4220. https://doi.org/10.1128/jvi.77.7.4205-4220.2003 PMID: 12634378

47. Gregory Bruce A, Barcy S, Dimaio T, Gan E, Jacques Garrigues H, Lagunoff M, et al. Quantitative analysis of the KSHV transcriptome following primary infection of blood and lymphatic endothelial cells. Pathogens. 2017;6. https://doi.org/10.3390/pathogens6010011 PMID: 28335496

48. Hu D, Wang V, Yang M, Abdullah S, Davis DA, Uldrick TS, et al. Induction of Kaposi's Sarcoma-Associated Herpesvirus-Encoded Viral Interleukin-6 by X-Box Binding Protein 1. J Virol. 2016; 90: 368–378. https://doi.org/10.1128/JVI.01192-15 PMID: 26491160

49. Wen KW, Damania B. Hsp90 and Hsp40/Erdj3 are required for the expression and anti-apoptotic function of KSHV K1. Oncogene. 2010; 29: 3532–3544. https://doi.org/10.1038/onc.2010.124 PMID: 20418907

50. Zhigang Z, Wuguo C, K SM, F BK, P DD, Blossom D. The K1 Protein of Kaposi's Sarcoma-Associated Herpesvirus Augments Viral Lytic Replication. J Virol. 2016; 90: 7657–7666. https://doi.org/10.1128/JVI.03102-15 PMID: 27307571

51. Wu J, Wu Y, Lian X. Targeted inhibition of GRP78 by HA15 promotes apoptosis of lung cancer cells accompanied by ER stress and autophagy. Biol Open. 2020;9. https://doi.org/10.1242/bio.053298 PMID: 33115703

52. Cancian L, Hansen A, Boshoff C. Cellular origin of Kaposi's sarcoma and Kaposi's sarcoma-associated herpesvirus-induced cell reprogramming. Trends in Cell Biology. 2013. pp. 421–432. https://doi.org/10.1016/j.tcb.2013.04.001 PMID: 23685018

53. Tuohinto K, DiMaio TA, Kiss EA, Laakkonen P, Saharinen P, Karnezis T, et al. KSHV infection of endothelial precursor cells with lymphatic characteristics as a novel model for translational Kaposi's sarcoma studies. PLoS Pathog. 2023;19. https://doi.org/10.1371/journal.ppat.1010753 PMID: 36689549

54. Chang HH, Ganem D. A unique herpesviral transcriptional program in KSHV-infected lymphatic endothelial cells leads to mTORC1 activation and rapamycin sensitivity. Cell Host Microbe. 2013; 13: 429–440. https://doi.org/10.1016/j.chom.2013.03.009 PMID: 23601105

55. Barrera MD, Callahan V, Akhrymuk I, Bhalla N, Zhou W, Campbell C, et al. Proteomic Discovery of VEEV E2-Host Partner Interactions Identifies GRP78 Inhibitor HA15 as a Potential Therapeutic for Alphavirus Infections. 2021. https://doi.org/10.3390/pathogens10030283 PMID: 33801554

56. Mao H, Palmer D, Rosenthal KS. Changes in BiP (GRP78) levels upon HSV-1 infection are strain dependent. Virus Res. 2001; 76: 127–135. https://doi.org/10.1016/s0168-1702(01)00257-x PMID: 11410313

57. Buchkovich NJ, Maguire TG, Yu Y, Paton AW, Paton JC, Alwine JC. Human cytomegalovirus specifically controls the levels of the endoplasmic reticulum chaperone BiP/GRP78, which is required for virion assembly. J Virol. 2008; 82: 31–39. https://doi.org/10.1128/JVI.01881-07 PMID: 17942541

58. Benboudjema L, Mulvey M, Gao Y, Pimplikar SW, Mohr I. Association of the Herpes Simplex Virus Type 1 Us11 Gene Product with the Cellular Kinesin Light-Chain-Related Protein PAT1 Results in the Redistribution of Both Polypeptides. J Virol. 2003; 77: 9192–9203. https://doi.org/10.1128/jvi.77.17.9192-9203.2003 PMID: 12915535

59. Vo M, Aguiar A, McVoy MA, Hertel L. Cytomegalovirus strain TB40/E restrictions and adaptations to growth in ARPE-19 epithelial cells. Microorganisms. 2020; 8. https://doi.org/10.3390/microorganisms8040615 PMID: 32344555

60. Zeh HJ, Downs-Canner S, McCart JA, Guo ZS, Rao UNM, Ramalingam L, et al. First-in-man study of western reserve strain oncolytic vaccinia virus: Safety, systemic spread, and antitumor activity. Molecular Therapy. 2015; 23: 202–214. https://doi.org/10.1038/mt.2014.194 PMID: 25292189

61. Yamamoto K, Yoshida H, Kokame K, Kaufman RJ, Mori K. Differential Contributions of ATF6 and XBP1 to the Activation of Endoplasmic Reticulum Stress-Responsive cis-Acting Elements ERSE, UPRE and ERSE-II. The Journal of Biochemistry. 2004; 136: 343–350. https://doi.org/10.1093/jb/mvh122 PMID: 15598891

62. Pakos-Zebrucka K, Koryga I, Mnich K, Ljujic M, Samali A, Gorman AM. The integrated stress response. EMBO Rep. 2016; 17: 1374–1395. https://doi.org/10.15252/embr.201642195 PMID: 27629041

63. Godet A-C, David F, Hantelys F, Tatin F, Lacazette E, Garmy-Susini B, et al. IRES Trans-Acting Factors, Key Actors of the Stress Response. Int J Mol Sci. 2019; 20: 924. https://doi.org/10.3390/ijms20040924 PMID: 30791615

64. Johannes G, Sarnow P. Cap-independent polysomal association of natural mRNAs encoding c-myc, BiP, and eIF4G conferred by internal ribosome entry sites. RNA. 1998; 4: S1355838298981080. https://doi.org/10.1017/s1355838298981080 PMID: 9848649

65. Yang Y, Wang Z. IRES-mediated cap-independent translation, a path leading to hidden proteome. Journal of Molecular Cell Biology. Oxford University Press; 2019. pp. 911–919. https://doi.org/10.1093/jmcb/mjz091 PMID: 31504667

66. Komar AA, Merrick WC. A Retrospective on eIF2A—and Not the Alpha Subunit of eIF2. Int J Mol Sci. 2020; 21: 2054. https://doi.org/10.3390/ijms21062054 PMID: 32192132

67. Hollien J, Lin JH, Li H, Stevens N, Walter P, Weissman JS. Regulated Ire1-dependent decay of messenger RNAs in mammalian cells. Journal of Cell Biology. 2009; 186: 323–331. https://doi.org/10.1083/jcb.200903014 PMID: 19651891

68. Li W, Okreglak V, Peschek J, Kimmig P, Zubradt M, Weissman JS, et al. Engineering ER-stress dependent non-conventional mRNA splicing. Elife. 2018; 7. https://doi.org/10.7554/eLife.35388 PMID: 29985129

69. Jenner RG, Maillard K, Cattini N, Weiss RA, Boshoff C, Wooster R, et al. Kaposi's sarcoma-associated herpesvirus-infected primary effusion lymphoma has a plasma cell gene expression profile. Proceedings of the National Academy of Sciences. 2003; 100: 10399–10404. https://doi.org/10.1073/pnas.1630810100 PMID: 12925741

70. Ma Y, Shimizu Y, Mann MJ, Jin Y, Hendershot LM. Plasma cell differentiation initiates a limited ER stress response by specifically suppressing the PERK-dependent branch of the unfolded protein response. Cell Stress Chaperones. 2010; 15: 281–293. https://doi.org/10.1007/s12192-009-0142-9 PMID: 19898960

71. Horibe T, Torisawa A, Kurihara R, Akiyoshi R, Hatta-Ohashi Y, Suzuki H, et al. Monitoring Bip promoter activation during cancer cell growth by bioluminescence imaging at the single-cell level. Integr Cancer Sci Ther. 2016;2. https://doi.org/10.15761/ICST.1000157

72. Kitajewski J, Mason JO, Varmus HE. Interaction of *Wnt-1* Proteins with the Binding Protein BiP. Mol Cell Biol. 1992; 12: 784–790. https://doi.org/10.1128/mcb.12.2.784–790.1992 PMID: 1531088

73. Hayward SD, Liu J, Fujimuro M. Notch and Wnt Signaling: Mimicry and Manipulation by Gamma Herpesviruses. Science's STKE. 2006; 2006. https://doi.org/10.1126/stke.3352006re4 PMID: 16705130

74. Lee AS, Brandhorst S, Rangel DF, Navarrete G, Cohen P, Longo VD, et al. Effects of Prolonged GRP78 Haploinsufficiency on Organ Homeostasis, Behavior, Cancer and Chemotoxic Resistance in Aged Mice. Sci Rep. 2017; 7. https://doi.org/10.1038/srep40919 PMID: 28145503